# Antiferromagnetic skyrmions in spintronics

Miina Leiviskä, Coline Thevenard, Carenza Cronshaw, Javier Rial, Sarah Jenkins, Daria Gusakova, Richard F. L. Evans, Vincent Baltz

Book chapter

# 15. Antiferromagnetic skyrmions in spintronics

**M. Leiviskä[1], C. Thevenard[1], C. Cronshaw[2], J. Rial[1,3], S. Jenkins[2], D. Gusakova[1], R. F. L. Evans[2], and V. Baltz[1,*]**

[1]Univ. Grenoble Alpes, CNRS, CEA, Grenoble INP, IRIG-SPINTEC, F-38000 Grenoble, France

[2]School of Physics, Engineering and Technology, University of York, York YO10 5DD, United Kingdom

[3]Univ. Autonoma Madrid, Dept. Fis. Mat. Condensada, E-28049 Madrid, Spain

[*]vincent.baltz@cea.fr

The following chapter starts from a base of fundamental physics and from this explains the major advantages that antiferromagnetic skyrmions can provide for applications.

## 1. Introduction (VB)

Topology is an important concept in physics, and therefore in spintronics, since it has unprecedented repercussions for most of the spin-dependent properties of materials, whether electrical, thermal or optical [Topology in Magnetism, J. Zang *et al* (eds), Springer Nature (2018)]. Topology can refer to either *global topology* where the topology is imposed by the symmetries of the periodic spin structure as described by the symmetry groups or to a *local topology* which is generated by a local deformation in the global topology. In this chapter, we will focus on local topology. One of the specificities of these deformations or topological objects is that they are *topologically protected*: it is not possible to recover the local topology by applying a stimulus in a continuous manner e. g. a magnetic field. Topological protection is true in the mathematical sense for a continuous object, but suffers in practice from the discretization naturally imposed by the atomic lattice, not to mention the many possible structural defects.

While topological objects in ferromagnetic materials, i.e. materials with an all-parallel spin lattice, have naturally been the most studied both from a fundamental point of view and for their possible applications [A. Soumyanarayanan *et al*, Nature **539**, 509 (2016); B. Göbel *et al*, Phys. Rep. **895**, 1 (2021)], the presence of several spin sub-lattices in antiferromagnetic and altermagnetic materials with zero net magnetization [T. Jungwirth *et al*, Nat. Nano. **11**, 231 (2016); V. Baltz *et al*, Rev. Mod. Phys. **90**, 015005 (2018)], opens up new perspectives in terms of topology and associated physical effects and spintronic applications [L. Smejkal et al, Phys. Rev. X **12**, 040501 (2022); V. Bonbien et al, J. Phys. D: Appl. Phys. **55**, 103002 (2022)].

The aim of this chapter is to review the specific features associated with the skyrmion topological object in antiferromagnetic materials, from the point of view of both magnetic and electrodynamic properties, in the context of possible applications.

## 2. Background on ferromagnetic skyrmions (VB)

Let us first recall how skyrmions in ferromagnets are described, used and how they influence electrodynamics. This will serve as a basis for a later comparison with their antiferromagnetic counterparts. Interested readers can find more information on skyrmions and beyond, in for example

the review articles A. Soumyanarayanan *et al*, Nature **539**, 509 (2016) and B. Göbel *et al*, Phys. Rep. **895**, 1 (2021), and references therein.

Description of a ferromagnetic skyrmion

The magnetic texture $\widehat{\boldsymbol{M}}$ of a two dimensional skyrmion is described mathematically by the spatial variation of the normalized magnetization density, which is expressed as :

$$\widehat{\boldsymbol{M}} = \begin{pmatrix} \sin\Theta(r)\cos\Phi(\phi) \\ \sin\Theta(r)\sin\Phi(\phi) \\ p_F\cos\Theta(r) \end{pmatrix} \quad (1)$$

where $r$ and $\phi$ are the radial distance and azimuthal angle [FIG. 1(a)] used to express the position of $\widehat{\boldsymbol{M}}$. $\Theta$ and $\Phi$ are the $r$-dependent polar and azimuthal angles, describing the orientation of $\widehat{\boldsymbol{M}}$. $p_F = \pm 1$ which is called the polarity. The polarity corresponds to the out-of-plane magnetization density of the core of the skyrmion. The in-plane magnetization density called vorticity is described by $\Phi = m_F\phi + \gamma_F$, where $m_F = 0, \pm 1, \pm 2, \ldots$ . Vorticity indicates the number of times the magnetization density has rolled up in-plane. $\gamma_F$ is an angle called the helicity which is continuous and describes the extent to which the winding of the magnetization density $\widehat{\boldsymbol{M}}$ lags behind the winding of the position $r$. For $\gamma_F = 0$, the in-plane component of $\widehat{\boldsymbol{M}}$ is radial and the skyrmion is of the Néel type, whereas, for $\gamma_F = \pi/2$, the in-plane component is tangential and the skyrmion is of the Bloch type.

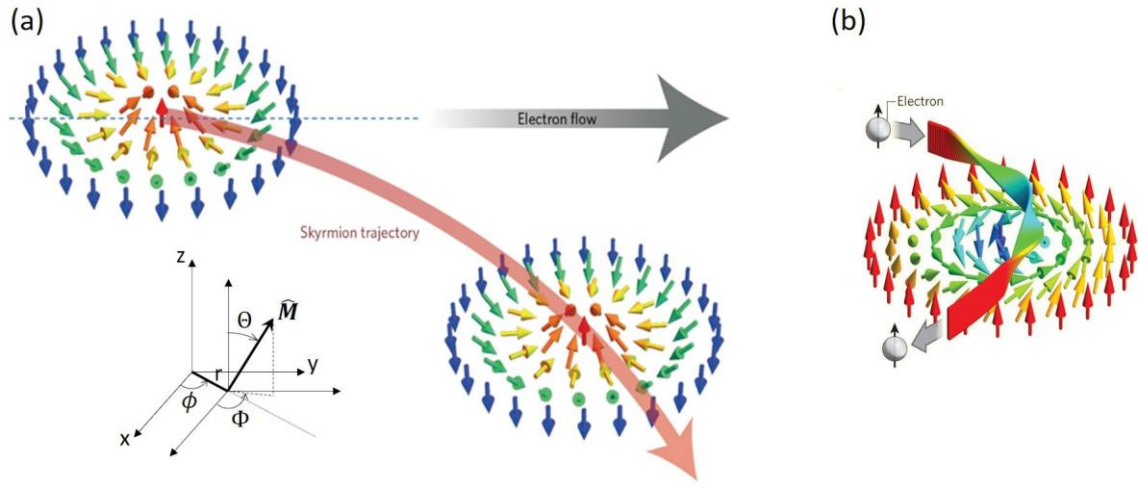


FIG. 1. (a) Illustration of the current-induced torque motion of a Néel-type skyrmion with $(p_F, m_F, \gamma_F) = (1,1,\pi)$, in which the skyrmion Hall effect deviates the skyrmion laterally from the electron flow. Adapted with permission from Springer Nature: G. Chen, Nat. Phys. **13**, 112 (2017). Copyright 2017. (b) Illustration of the reciprocal topological Hall effect, in which the skyrmion, here with $(p_F, m_F, \gamma_F) = (-1,-1,\pi/2)$, deflects the trajectory of the electrons. Reprinted with permission from Springer Nature: C. Pfleiderer & A. Rosch, Nature **465**, 880 (2010). Copyright 2010.

The magnetic texture of a skyrmion formulated by Eq. (1) is the result of the balance between the different magnetic interactions of the system and the resulting energies. These include the short-range exchange interaction between the magnetic moments (typically a few $10^{-21}$ $J$ per pair of moments), which favors parallel or antiparallel alignment, the short-range chiral Dzyaloshinskii–Moriya (DMI)

interaction, be it bulk like in the B20 phase of MnSi, MnGe, and FeCoSi, or interfacial, like in Pt/Co and Fe/Ir heterostructures (a few $10^{-4}\,J.m^{-2}$ for the *volumetric* DMI), which favors some canting - typically giving rise to small Néel-type skyrmions (< 100 nm), and the long-range achiral dipolar interaction, which can also yield some canting, typically forming larger skyrmions of the Bloch type. Note that the original works on DMI were performed on some antiferromagnets where bulk-DMI induces some canting [I. E. Dzyaloshinskii, J. Phys. Chem. Solid. **4**, 241 (1958); T. Moriya, Phys. Rev. **120**, 91 (1960)]. Examples of canted antiferromagnets are hematite $Fe_2O_3$ above the Morin transition, and several rare-earth orthoferrites $RFeO_3$ with R=Y,Ho,Dy.

Polarity $p_F$, vorticity $m_F$ and helicity $\gamma_F$, whose values are governed by the balance of the energies in the system, are the three essential quantities not only for describing the magnetic texture of a skyrmion but also its motion and its influence on the electrodynamic properties of electron flow.

Note that the topological index $Q_F$,

$$Q_F = \frac{1}{4\pi}\int \widehat{\boldsymbol{M}} \cdot \left(\partial_x \widehat{\boldsymbol{M}} \times \partial_y \widehat{\boldsymbol{M}}\right) dxdy = p_F m_F \qquad (2)$$

which describes the topology of the system and depends only on $p_F$ and $m_F$, will naturally influence the dynamic properties of a skyrmion and electrons flowing through a skyrmion. We must not forget that the helicity $\gamma_F$ will also have an influence, albeit in a different way, especially as it can break the rotational symmetry of the skyrmion.

Description of current-induced motion of a ferromagnetic skyrmion

Considering a steady and rigid behavior, the in-plane $(x, y)$ motion of the center of mass of a skyrmion with velocity $\boldsymbol{v}$ is best described by a modified Thiele equation. It is derived from the known Landau–Lifshitz–Gilbert (LLG) equation which accounts for transport specific effects such as the forces arising from the Berry phase that electrons pick up when their spins adiabatically follow the topology of the magnetization density in the skyrmion [FIG. 1(b)]. Detailed calculations showing how the transport-specific effects for a skyrmion are included in the LLG equation can for example be found in K. Everschor *et al*, Phys. Rev. B **86**, 054432 (2012). The Thiele equation thus reads:

$$\boldsymbol{G} \times \boldsymbol{v} - \alpha \overline{\overline{D}} \cdot \boldsymbol{v} + \boldsymbol{F} = 0 \qquad (3)$$

The first term in the equation describes the topological Magnus force. For a Néel-type two-dimensional skyrmion one gets $\boldsymbol{G} = -4\pi Q_F \hat{\boldsymbol{z}}$, known as the gryromagnetic coupling vector, indeed related to the skyrmion topological index $Q_F$, and therefore to the polarity $p_F$ and vorticity $m_F$ [Eq. (2)]. The second term represents the dissipative force which is governed by the dyadic tensor $\overline{\overline{D}}$, with $D_{ij} = \iint \left(\partial_i \widehat{\boldsymbol{M}} \cdot \partial_j \widehat{\boldsymbol{M}}\right) dxdy$. The last term is the force $\boldsymbol{F}$ at the origin of the motion, i. e. due to 'electron-skyrmion coupling' for current-induced motion. For the case of a current-induced spin torque, it writes $\boldsymbol{F} = 4\pi \overline{\overline{B}} \cdot J_e \hat{\boldsymbol{s}}$, where $\overline{\overline{B}}$ is a tensor related to an emergent topological magnetic flux density, with $B_{ij} = \iint \left(\partial_i \widehat{\boldsymbol{M}} \times \widehat{\boldsymbol{M}}\right)_j dxdy$, $J_e$ is the charge current, applied for example in the ferromagnetic layer or in an adjacent non-magnetic layer, and $\hat{\boldsymbol{s}}$ is the normalized polarization of the electron spin. For example, in the case of a spin Hall effect-induced spin-orbit torque in a ferromagnet/non-magnet bilayer, the transverse spin current initiating the torque at the ferromagnet/non-magnet interface is $J_s^0 = \theta_{SHE} \eta J_e$. It flows along $\hat{\boldsymbol{z}}$ in FIG. 1(b), with $\hat{\boldsymbol{s}} = \hat{\boldsymbol{x}}$, and is associated to a longitudinal charge current $\boldsymbol{J}_e$, along $\hat{\boldsymbol{y}}$ in FIG. 1(b). $\theta_{SHE}$ is the spin Hall angle accounting for the spin-orbit related charge current

to spin current conversion, and $\eta$ is a parameter resulting from spin accumulation, which takes into account: i) spin flip process in the non-magnetic layer, i. e. that only a fraction of the converted spin current matters as the conversion far from the interface will be depolarized by the time it reaches the interface, and ii) the efficiency of the transfer of angular momentum, through the spin mixing conductance $g^{\uparrow\downarrow}$. Interested readers can find more information on the anomalous Hall and reciprocal spin Hall effects, in the review article of N. Nagaosa *et al*, Rev. Mod. Phys. 82, 1539 (2010), and references therein, see also the textbook of V. Baltz, The basics of electron transport in spintronics, EDP Sciences, ISBN-978-2-7598-2917-0_(2023), and references therein.

We note that, for a better comparison with antiferromagnetic skyrmions dynamics, which we will describe in the next parts, Eq. (3) can also be formulated in terms of collective coordinates $\boldsymbol{b}(t) = \{b_0, b_1, \dots, b_n\}$, so that $\widehat{\boldsymbol{M}}(\boldsymbol{r}, t) = \widehat{\boldsymbol{M}}\big(\boldsymbol{r}, \boldsymbol{b}(t)\big)$ [O. A. Tretiakov *et al*, Phys. Rev. Lett. **100**, 127204 (2008)], giving

$$G^{ij}\dot{b}_j + \alpha\Gamma^{ij}\dot{b}_j + F^i = 0 \qquad (4)$$

where $G^{ij}$ and $\Gamma^{ij}$ are the matrix elements of the gyromagnetic and damping tensors, and $F^i$ are the components of the force vector. There is an infinite number of collective coordinates, but only a very small finite number of collective coordinates, a. k. a. soft modes, like position and angle, suffice to describe the system. These parameters have long relaxation times and they are treated as dynamic parameters. All other parameters, a. k. a. hard modes like skyrmion size, adjust adiabatically to their relaxation value and can be discarded as dynamic parameters.

One of the messages in Eqs. (3) and (4) is that the trajectory of a skyrmion can deviate from a straight line. For example, for electrons flowing along $\hat{\boldsymbol{y}}$ through the Néel-type skyrmion of FIG. 1(a), with $(p_F, m_F, \gamma_F) = (1,1,0)$, it can be shown from Eqs. (1-3) that the deviation of the trajectory is: $\frac{v_x}{v_y} = -\frac{Q}{\alpha D}$, with $D = D_{xx} = D_{yy}$ and $D_{xy} = D_{yx} = 0$ [W. Jiang *et al*, Nat. Phys. **13**, 162 (2017)]. This effect is known as the skyrmion Hall effect [FIG. 1(a)]. It is undesirable in planned spintronic applications, such as in a skyrmion-based racetrack memory, where the skyrmion Hall effect will lead to limitations in the propagation of spin information, as the skyrmions would annihilate at the edges of the track after a certain distance. In practice, typical values are $v_x/v_y \approx 0.25$ for a current density $J_e \approx 5 \times 10^6\ A.cm^{-2}$ ($v_x \approx 0.5\ m.s^{-1}$), corresponding to a skyrmion Hall angle $\phi_{Sk} = \tanh^{-1}\big(v_x/v_y\big) \approx 15°$.

There are several ways of mitigating the skyrmion Hall effect. We present three of them below.

Firstly, it is possible to fine shaping the direction of the external torque force through $\hat{\boldsymbol{s}}$ by modifying the geometry of the device and heterostructure so that $\boldsymbol{F}$ compensates for $\boldsymbol{G} \times \boldsymbol{v}$.

A second possible way is engineering the skyrmion's texture, as this is a possible lever for adjusting the forces $\boldsymbol{F}$ and $\boldsymbol{G} \times \boldsymbol{v}$ relative to each other. Indeed, although Eq. (3) relegates the motion of the skyrmion to the motion of its centre of mass, it should be noted that the subtle influence of the skyrmion's magnetic texture on motion is included in the parameters $\boldsymbol{G}$, $\overline{\overline{D}}$, and $\overline{\overline{B}}$. For example it is possible to show that $\overline{\overline{B}}$ depends on helicity $\gamma_F$ and that in some cases, a $\gamma_F$-dependent transversal force $\boldsymbol{F}(\gamma_F)$ can be generated. In these cases, it can be simplified to say that the torque acting on either side of the centre of the skyrmion will not compensate because $\gamma_F$ breaks the rotational symmetry that imposes compensation otherwise.

A third possible solution for mitigating the skyrmion Hall effect is to use assimilated topological objects for which the transverse forces are assumed to be self-compensating like a synthetic antiferromagnetic skyrmion, i. e. composed of two antiferromagnetically coupled skyrmions in two separate ferromagnetic layers or skyrmions in antiferromagnetic materials, i. e. antiferromagnetic skyrmions. An antiferromagnet is made of several imbricated and strongly exchange coupled magnetic sub-lattices that have zero net magnetization. A prototypical antiferromagnetic skyrmion thus consists of several imbricated and strongly coupled skyrmions verifying zero net polarity, vorticity and helicity, if transposed in the ferromagnets' frame. Antiferromagnetic skyrmions are the main focus of this article, all the more so as their longitudinal skyrmion velocity due to the inherent THz dynamics in antiferromagnets exceeds that of the ferromagnetic skyrmions, which obey GHz dynamics. The veracity of prototypical antiferromagnetic skyrmions and the specific characteristics associated with them, from the point of view of magnetic and electrodynamic properties, will be introduced in §3 and detailed in the following sections.

With regard to skyrmion motion, we note here that a skyrmion is not necessarily a two-dimensional object, but may well extend along the third dimension, ie. in the form of a tube called a tubular skyrmion or a bubble called a bobbler. The fine texture of the skyrmion along the third dimension will certainly influence its motion and modify the fine tuning anticipated in two-dimensions for mitigating the skyrmion Hall effect. We also note that some pinning on defects or certain spin torque geometries can modify the morphology of the skyrmion, thus influencing its motion which needs to be taken into account.

Influence of a ferromagnetic skyrmion on electrodynamics

Naturally, in a reciprocal way, the forces absorbed by the electron due to the Berry phase when their spin adiabatically follows the topology of the magnetisation density in the skyrmion will deflect the electron flow that interacts with the skyrmion. This is known as the topological Hall effect. In addition to the topological Hall effect, which may not necessarily be zero in all antiferromagnets [B. Göbel *et al*, Phys. Rev. B **96**, 060406(R) (2017)], other predicted effects of antiferromagnetic skyrmions on the transport properties include the nonvanishing topological spin Hall effect [P. M. Buhl *et al*, Phys. Status Solidi RRL **11**, 1700007 (2017); C. Akosa *et al*, Phys. Rev. Lett. **121**, 097204 (2018)]. These properties make antiferromagnetic skyrmions not only fascinating candidates as competitive information carriers for ultra-dense, ultra-fast, low-power spintronic devices [H. Xia *et al*, J. Phys. D: Appl. Phys. **50**, 505005 (2017); X. Zhao *et al*, Appl. Phys. Lett. **112**, 252402 (2018); R L Silva *et al*, J. Phys.: Condens. Matter **31** 225802 (2019); X. Liang *et al*, Phys. Rev. B **100**, 144439 (2019) ; X. Liang *et al*, Phys. Rev. B **100**, 144439 (2019); L. Shen *et al*, Appl. Phys. Lett. **114**, 042402 (2019); X. Liang *et al*, Appl. Phys. Lett. **119**, 062403 (2021) ; P. E. Roy, J. Appl. Phys. **129**, 193902 (2021) ; N. Bindal *et al*, Nanotechnol. **32**, 215204 (2021); N. Bindal *et al*, J. Phys. D: Appl. Phys. **55** 345007 (2022) ; R. L.Silva *et al*, Phys. Lett. A **425**, 127868 (2022); N. Bindal *et al*, Nanoscale Adv. **5**, 450 (2023)] but also for studies on topology.

## 3. Formalism to describe an antiferromagnetic skyrmion, its motion and the associated elecrodynamics (VB)

The aim of this section is to provide a simple framework for understanding the main differences between ferromagnetic and antiferromagnetic skyrmions. This section will serve as a frame of reference for the following sections, in which some of the concepts will be explained in greater detail. Interested readers can find complementary information in the following review articles, and references therein: V. Baltz *et al*, Rev. Mod. Phys. **90**, 015005 (2018); O. Gomonay *et al*, Nat. Phys. **14**, 213 (2018); B. Göbel *et al*, Phys. Rep. **895**, 1 (2021); L. Shen et al chap. 13 in: E. Kamenetskii (ed)

Chirality, Magnetism and Magnetoelectricity, Topics in Appl. Phys. **138**, Springer, Cham (2021); V. Bonbien et al, J. Phys. D: Appl. Phys. **55**, 103002 (2022).

Description of an antiferromagnetic skyrmion

In the simplest case, which consists of a collinear bipartite antiferromagnet, like NiO, $Mn_2Au$, $Fe_2O_3$ below the Morin temperature, $Cr_2O_3$, CuMnAs, and $Mn_5Ge_3$. The antiferromagnet is described using two vectors: the order parameter $\hat{\boldsymbol{L}}$, a. k. a. the Néel vector, and the net magnetisation $\hat{\boldsymbol{M}}_{net}$, such that

$$\hat{\boldsymbol{L}} = \left(\hat{\boldsymbol{M}}_{\boldsymbol{1}} - \hat{\boldsymbol{M}}_{\boldsymbol{2}}\right)/2 \tag{5}$$

$$\hat{\boldsymbol{M}}_{net} = \left(\hat{\boldsymbol{M}}_{\boldsymbol{1}} + \hat{\boldsymbol{M}}_{\boldsymbol{2}}\right)/2 \tag{6}$$

$\hat{\boldsymbol{M}}_{\boldsymbol{1}}$ and $\hat{\boldsymbol{M}}_{\boldsymbol{2}}$ are the normalized magnetization density of the two sub-lattices, which are antiferromagnetically coupled through the internal exchange field $H_E$. Of course, by definition, $\hat{\boldsymbol{M}}_{net}$ and $\hat{\boldsymbol{L}}$ are indissolubly linked, meaning for example that a change of $\hat{\boldsymbol{M}}_{net}$ provokes a change of $\hat{\boldsymbol{L}}$.

The magnetic texture of a two-dimensional antiferromagnetic skyrmion is then described in exactly the same way as for a ferromagnet, by replacing $\hat{\boldsymbol{M}}$ by $\hat{\boldsymbol{L}}$ in Eq. (1), provided that the inter-sub-lattice exchange term, $H_E$, dominates all the other terms like anisotropy and DMI [X. Ma *et al*, Phys. Rev. Lett. **119**, 027202 (2017); R. A. Khan *et al*, Phys. Rev. B **98**, 064413 (2018); Md. R. K. Akanda *et al*, Phys. Rev. B **102**, 224414 (2020); Y. Q. Guo *et al*, J. Magn. Magn. Mater. 572, 170594 (2023)], thus rigidly aligning pairs of antiparallel moments [FIG. 2(a)]. As a result, at equilibrium, $\hat{\boldsymbol{M}}_{net} = 0$ and

$$\hat{\boldsymbol{L}} = \begin{pmatrix} \sin\Theta(r)\cos\Phi(\phi) \\ \sin\Theta(r)\sin\Phi(\phi) \\ p_{AF}\cos\Theta(r) \end{pmatrix} \tag{7}$$

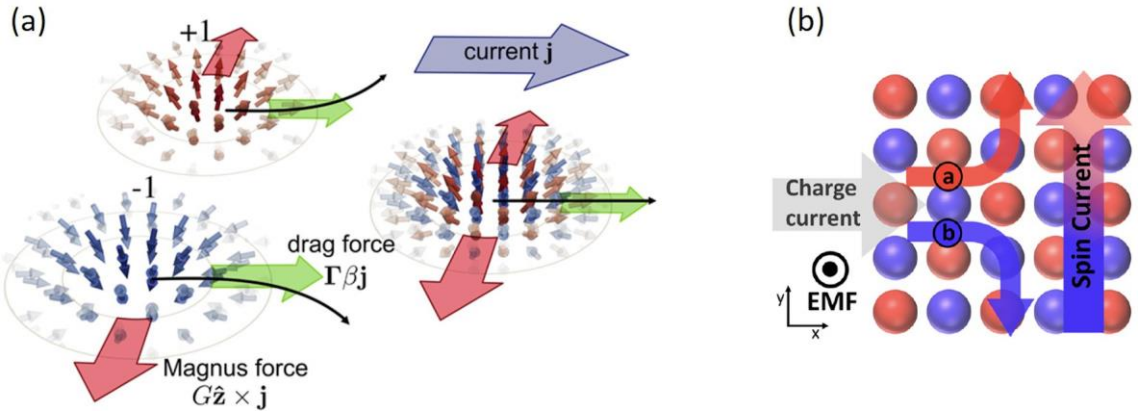


FIG. 2. (a) Illustration of a skyrmion in a collinear bipartite antiferromagnet, made of two exchange coupled intertwined ferromagnetic skyrmions, and its current-induced motion for which the skyrmion Hall effect is mitigated for the simplest case. Reprinted with permission from the American Physical Society: J. Barker & O. Tretiakov, Phys. Rev. Lett. **116**, 147203 (2016). Copyright 2016. (b) Illustration of the topological spin Hall effect impacting electron dynamics, as a result of coupling with the topology of the antiferromagnetic skyrmion creating an "emergent magnetic field" (EMF). Reprinted with permission from the American Physical Society: C. Akosa *et al*, Phys. Rev. Lett. **121**, 097204 (2018). Copyright 2018.

In the same way, polarity $p_{AF}$, vorticity $m_{AF}$ and helicity $\gamma_{AF}$, are the three essential quantities for describing the magnetic texture of an antiferromagnetic skyrmion. The topological index of this type of object is also described by Eq. (2), by replacing $\widehat{\boldsymbol{M}}$ with $\hat{\boldsymbol{L}}$, such that

$$Q_{AF} = \frac{1}{4\pi}\int \hat{\boldsymbol{L}} \cdot \left(\partial_x \hat{\boldsymbol{L}} \times \partial_y \hat{\boldsymbol{L}}\right) dxdy = p_{AF} m_{AF} \tag{8}$$

Description of current-induced motion of an antiferromagnetic skyrmion

When the magnetic texture of the simplest antiferromagnetic and ferromagnetic skyrmions can be described in a similar manner, the dynamics of the order parameter significantly differs. This is especially true for an antiferromagnetic skyrmion as it is governed by the strong exchange coupling, $H_E$, between the two sub-lattices. In fact, a slight canting between the moments of the two sub-lattices, initiated in the first instance, leads to a significant reaction in the second instance, as the moments of one sub-lattice are then subjected to the torque created by the exchange field of the other sub-lattice. The motion of an antiferromagnetic skyrmion is therefore in the THz range, as the exchange field, $H_E$, is several orders of magnitude greater than the terms such as anisotropy and dipolar fields that usually govern ferromagnetic dynamics, which is in the GHz range. It is important to note that not only are the dynamic of an antiferromagnetic skyrmion several orders of magnitude faster than that of its ferromagnetic counterpart, but also that it does not follow the same kinetics because it is inertial. It is also said to be Newtonian or second order [Eq. (9)].

The motion of an antiferromagnetic skyrmion can indeed be described, in terms of collective coordinates, so that $\hat{\boldsymbol{L}}(\boldsymbol{r}, t) = \hat{\boldsymbol{L}}\left(\boldsymbol{r}, \boldsymbol{b}(t)\right)$ [E. G. Tveten *et al*, Phys. Rev. Lett. **110**, 127208 (2013)]:

$$\mathcal{M}^{ij}\ddot{b}_j + \alpha\mathcal{T}^{ij}\dot{b}_j + \mathcal{F}^i = 0 \tag{9}$$

where $\mathcal{M}^{ij}$ and $\mathcal{T}^{ij}$ are the matrix elements of some mass and damping tensors, and $\mathcal{F}^i$ is the component of the force vector, which includes the internal exchange force, the current induced force, and the external field force. These matrix elements and vector components are detailed in E. G. Tveten *et al*, Phys. Rev. Lett. **110**, 127208 (2013).

Compared to the motion of a ferromagnetic skyrmion [Eq. (4)], the first term in Eq. (9) is new and specific to antiferromagnets. It accounts for some inertia and arises from the inter-sub-lattice exchange interaction, $H_E$. Note that steady state dynamics are reached after a few picoseconds. Another difference between ferromagnetic [Eq. (4)] and antiferromagnetic [Eq. (9)] skyrmion dynamics is the absence of the gyromagnetic force for the simplest antiferromagnets mitigating the skyrmion Hall effect and making the trajectory straight [FIG. 2(a)]. Indeed, for the ideal case of a collinear bipartite antiferromagnet, the gyroforce of one sub-lattice opposes the one of the other sub-lattice: $G_1^{ij} = -G_2^{ij}$ [Eq. (4)] and the net gyroforce cancels out: $G^{ij} = 0$ [J. Barker and O. Tretiakov, Phys. Rev. Lett. **116**, 147203 (2016)]. Calculations [R. Msiska *et al*, Phys. Rev. Appl. **17**, 064015 (2022)] show that the ideal case where an antiferromagnetic skyrmion evolves on a straight line is not necessarily obtained however because some torques initiating motion, included in the term $\mathcal{F}^i$ in Eq. (9), can possess some transverse components these may not cancel out, especially when the helicity $\gamma_{AF}$ is non-zero (see §2).

More complicated magnetic orders, beyond collinear bipartite antiferromagnets [I. Raicevic *et al*, Phys. Rev. Lett. **106**, 227206 (2011); J. Barker and O. Tretiakov, Phys. Rev. Lett. **116**, 147203 (2016); J.

Harrison *et al*, Phys. Rev. B **105**, 224424 (2022); O. J. Amin *et al*, Nature Nanotech. **18**, 849 (2023)] may also host antiferromagnetic skyrmions. In this case a complete description needs to be developed as the order parameter can no longer be described by $\hat{\boldsymbol{L}}$ and $\widehat{\boldsymbol{M}}_{net}$ [Eqs (5) and (6)]. For example, the macroscopic magnetization in noncollinear antiferromagnets is framed by cluster multipole moments [M.-T. Suzuki *et al*, Phys. Rev. B **95**, 094406 (2017)]. For example in typical 3Q magnetic phases such as $Mn_3X$ (X = Ir, Mn, Sn, Ge) antiferromagnets there are eight octupoles which point perpendicular to the eight equivalent (111) planes [H. D. Rosales *et al*, Phys. Rev. B **92**, 214439 (2015); K. G. Rana *et al*, Appl. Phys. Lett. **119**, 192407 (2021); X. Liu *et al*, Adv. Mater. **35**, 2211634 (2023); M. Leiviskä *et al*, Phys. Rev. B 108, 184424 (2023)]. An extension to cycloidal antiferromagnetic order, where topological defects have been observed for example at the surface of bulk $BiFeO_3$ would also be interesting [J.-Y. Chauleau *et al*, Nat. Phys. **19**, 386 (2020); A. Finco *et al*, Phys. Rev. Lett. **128**, 187201 (2022)]. More information on the types of materials that favor the formation of antiferromagnetic skyrmions and the means of creating them will be given in §4 [I. Raicevic *et al*, Phys. Rev. Lett. **106**, 227206 (2011); H. D. Rosales *et al*, Phys. Rev. B **92**, 214439 (2015); X. Zhang *et al*, Sci. Rep. **6**, 24795 (2016); R Khoshlahni *et al*, Phys. Rev. B **99**, 054423 (2019); X. Xu *et al*, Phys. Rev. Appl. **11**, 024051 (2019) ; K. G. Rana *et al*, Appl. Phys. Lett. **119**, 192407 (2021); K. I. A. Khan *et al*, Sci. Rep. **11**, 12332 (2021) ; H. Belrhazi *et al*, Sci. Rep. **12**, 15226 (2022); R. L. Silva *et al*, Phys. Lett. A 448, 128328 (2022); A. Mukherjee *et al*, Phys. Rev. B **105**, 075102 (2022) ; J.-Y. Chauleau *et al*, Nat. Phys. **19**, 386 (2020); A. Finco *et al*, Phys. Rev. Lett. **128**, 187201 (2022) ; F. P. Chmiel *et al*, Nat. Mater. 17, 581 (2018) ; H. Jani *et al*, Nature **590**, 74 (2021) ; O. J. Amin *et al*, Nature Nanotech. **18**, 849 (2023); X. Liu *et al*, Adv. Mater. **35**, 2211634 (2023); M. Leiviskä *et al*, Phys. Rev. B 108, 184424 (2023); . K. C. Tan *et al*, Nat. Mater. (2023)]. It is important to mention here that, although there are many theoretical papers on the subject, the experimental work is very fragmented, for reasons that will be detailed in §4, making experimental nucleation of antiferromagnetic skyrmion in thin films the priority milestone.

Describing the motion of antiferromagnetic skyrmions [E. G. Tveten *et al*, Phys. Rev. Lett. **110**, 127208 (2013) ; X. Zhang *et al*, Sci. Rep. **6**, 24795 (2016) ; H. Velkov *et al*, New J. Phys. **18**, 075016 (2016) ; C. Jin *et al*, Appl. Phys. Lett. **109**, 182404 (2016); R. Zarzuela *et al*, Phys. Rev. B **97**, 014418 (2018) ; L. Shen *et al*, Phys. Rev. B **98**, 134448 (2018) ; L. Shen *et al*, Phys. Rev. Appl. **12**, 064033 (2019) ; L. Qiu *et al*, J. Magn. Magn. Matter **796**, 165922 (2020); S. Komineas and N. Papanicolaou, SciPost Phys. **8**, 086 (2020); H. Belrhazi *et al*, Sci. Rep. **12**, 15226 (2022); M. K. Wen *et al*, Phys. Rev. E **106**, 044137 (2022); S. Li *et al*, Phys. Rev. B **107**, 174409 (2023); R. Khoshlahni *et al*, Phys. Rev. B **107**,144421 (2023); R. V. Ovcharov *et al*, arXiv:2311.18583], we can make the same remarks as the motion of ferromagnetic skyrmions concerning the importance of the third dimension, defects and certain spin torque geometries. These can modify the morphology of the antiferromagnetic skyrmion or mitigate the forces acting on it, influencing its motion [H. Xia *et al*, J. Phys. D: Appl. Phys. **50**, 505005 (2017) ; C. Akosa *et al*, Phys. Rev. Lett. **121**, 097204 (2018) ; R. M. Menezes *et al*, Phys. Rev. B **99**, 104409 (2019) ; R L Silva *et al*, J. Phys.: Condens. Matter **31** 225802 (2019); X. Liang *et al*, Phys. Rev. B **100**, 144439 (2019) ; Z. Jin *et al*, Phys. Rev. B **102**, 054419 (2020) ; A. Salimath *et al*, Phys. Rev. B **101**, 024429 (2020) ;D. Toscano *et al*, J. Appl. Phys. **127**, 193902 (2020) ; M. N. Potkina *et al*, J. Appl. Phys. **127**, 213906 (2020); P. E. Roy, J. Appl. Phys. **129**, 193902 (2021); K. V. Yershov *et al*, Phys. Rev. B **105**, 054425 (2022); E. A. Tremsina and G. S. D. Beach, Phys. Rev. B **106**, L220402 (2022)]. These points will be examined in more detail in §5, along with the various methods that can be used to move an antiferromagnetic skyrmion.

Influence of an antiferromagnetic skyrmion on electrodynamics

The influence of an antiferromagnetic skyrmion on electrodynamics has long been hampered by the incorrect belief that a collinear bipartite antiferromagnetic skyrmion does not exhibit a net skyrmion

Hall effect and therefore would not cause a reciprocal topological Hall effect, although a topological spin Hall effect is possible [FIG. 2(b)] [P. M. Buhl *et al*, Phys. Status Solidi RRL **11**, 1700007 (2017); C. Akosa *et al*, Phys. Rev. Lett. **121**, 097204 (2018)]. Calculations [R. Msiska *et al*, Phys. Rev. Appl. **17**, 064015 (2022)] have demonstrated that antiferromagnetic skyrmions can exhibit a net skyrmion Hall effect and that a collinear bipartite antiferromagnetic skyrmion crystal with non-equivalent sub-lattice sites can exhibit a non-zero topological Hall effect [B. Göbel *et al*, Phys. Rev. B **96**, 060406(R) (2017)], meaning skyrmions are electrically detectable for use in spintronic devices. A more detailed description of the way in which an antiferromagnetic skyrmion can be detected, not only electrically [I. Raicevic *et al*, Phys. Rev. Lett. **106**, 227206 (2011); R. Cheng and Q. Niu, Phys. Rev. B **86**, 245118 (2012); O. Gomonay, Phys. Rev. B **91**, 144421 (2015);P. M. Buhl *et al*, Phys. Status Solidi RRL **11**, 1700007 (2017); C. Akosa *et al*, Phys. Rev. Lett. **121**, 097204 (2018); B. Göbel *et al*, Phys. Rev. B **96**, 060406(R) (2017); M. W. Daniels *et al*, Phys. Rev. B **99**, 224433 (2019); N. Djavid and R. K. Lake, Phys. Rev B **102**, 024419 (2020)] but also magnetically and optically [J.-Y. Chauleau *et al*, Nat. Phys. **19**, 386 (2020); A. Finco *et al*, Phys. Rev. Lett. **128**, 187201 (2022) ; K. G. Rana *et al*, Appl. Phys. Lett. **119**, 192407 (2021); O. J. Amin *et al*, Nature Nanotech. **18**, 849 (2023)], will be the subject of §6.

We remark here that, although the motion of a skyrmion and its influence on electron dynamics are closely related, the order parameter in coordinate space used to describe motion is not necessarily relevant for describing electron dynamics, as we recently learned from the lesson of altermagnetism [L. Smejkal et al, Phys. Rev. X **12**, 040501 (2022)]. Actually, while for both a collinear bipartite antiferromagnet and a collinear bipartite altermagnet, the Néel vector is sufficient to describe magnetism in coordinate space, it is no longer sufficient to describe electronic properties governed by the band structures in reciprocal momentum space. The bands are degenerate and no longer break time inversion in momentum space for antiferromagnets, whereas they are staggered and non-degenerate for altermagnets, breaking the time inversion in momentum space and opening new perspectives for electrodynamics in spintronics.

## 4. Nucleating antiferromagnetic skyrmions: magnetic, electrical, thermal and optical techniques (ML, CT)

In this section, we discuss how antiferromagnetic skyrmions can be created in real systems [I. Raicevic *et al*, Phys. Rev. Lett. **106**, 227206 (2011); H. D. Rosales *et al*, Phys. Rev. B **92**, 214439 (2015); X. Zhang *et al*, Sci. Rep. **6**, 24795 (2016); R Khoshlahni *et al*, Phys. Rev. B **99**, 054423 (2019); X. Xu *et al*, Phys. Rev. Appl. **11**, 024051 (2019); K. G. Rana *et al*, Appl. Phys. Lett. **119**, 192407 (2021); K. I. A. Khan *et al*, Sci. Rep. **11**, 12332 (2021); H. Belrhazi *et al*, Sci. Rep. **12**, 15226 (2022); R. L. Silva *et al*, Phys. Lett. A **448**, 128328 (2022); A. Mukherjee *et al*, Phys. Rev. B **105**, 075102 (2022); A. Finco *et al*, Phys. Rev. Lett. **128**, 187201 (2022); J.-Y. Chauleau *et al*, Nat. Phys. **19**, 386 (2020); F. P. Chmiel *et al*, Nat. Mater. 17, 581 (2018) ; H. Jani *et al*, Nature **590**, 74 (2021); O. J. Amin *et al*, Nature Nanotech. **18**, 849-853 (2023); X. Liu *et al*, Adv. Mater. **35**, 2211634 (2023); M. Leiviskä *et al*, Phys. Rev. B **108**, 184424 (2023); . K. C. Tan *et al*, Nat. Mater. (2023)]. Controlled and reproducible nucleation of antiferromagnetic skyrmions is a critical step in further investigations of their properties as well as in their implementation in practical applications. Controlling the order parameter of compensated magnets, however, is not trivial due to it being weakly sensitive to external field perturbations. Therefore, the experimental observations of antiferromagnetic skyrmions are thus far limited. Here, we will consider nucleation techniques relying on three distinct physical processes: i) field-assisted [I. Raicevic *et al*, Phys. Rev. Lett. **106**, 227206 (2011); H. D. Rosales *et al*, Phys. Rev. B **92**, 214439 (2015); A. Mukherjee *et al*, Phys. Rev. B **105**, 075102 (2022); S. Muhlbauer *et al*, Science **323**, 915-919 (2009); W. Munzer *et al*, Phys. Rev. B **81**, 041203(R) (2010); S. Hayami, Phys. Rev. B **105**, 014408 (2022); R.L. Silva *et al*, Phys. Lett. A **448**,

128328 (2022); J.-Y. Chauleau *et al*, Nat. Phys. **19**, 386 (2020); F. P. Chmiel *et al*, Nat. Mater. 17, 581 (2018) ; H. Jani *et al*, Nature **590**, 74 (2021); S. Gao *et al*, Nature **586**, 37 (2020); M. Leiviskä *et al*, Phys. Rev. B **108**, 184424 (2023); G. Salazar-Alvarez *et al*, Appl. Phys. Lett. **95**, 012510 (2009); J. Wu *et al*, Nat. Phys. **7**, 303 (2011); K.G. Rana *et al*, Appl. Phys. Lett. **119**, 192407 (2021); J. Nogues *et al*., J. Magn. Mag. Mat. 192 203 (1999) ; . K. C. Tan *et al*, Nat. Mater. (2023)], ii) electrical [X. Zhang *et al*, Sci. Rep. **6**, 24795 (2016) ; C. Jin *et al*, Appl. Phys. Lett. **109**, 182404 (2016); K.I.A. Khan *et al*, Sci. Rep. **11**, 12332 (2021); H. Belrhazi *et al*, Sci. Rep. **12**, 15226 (2022); O. J. Amin *et al*, Nature Nanotech. **18**, 849-853 (2023); X. Xu *et al*, Phys. Rev. Appl. **11**, 024051 (2019); T. Jungwirth *et al*, Nature Nanotech. **11**, 231 (2016); V. Baltz *et al*, Rev. Mod. Phys. **90**, 015005 (2018); R. Khoshlahni *et al*, Phys. Rev. B **99**, 054423 (2019)], and iii) thermal and optical [S.-G. Je *et al*, Nano Lett. **18**, 7362 (2018); G. Berruto *et al*, Phys. Rev. Lett. **120**, 117201 (2018); R. Juge *et al*, Nature Commun. **13**, 4807 (2022); R. Khoshlahni *et al*, Phys. Rev. B **99**, 054423 (2019); V. Flovik *et al*, Phys. Rev. B **96**, 140411(R) (2017); O.J. Amin *et al*, Nature Nanotech. **18**, 849 (2023) and A. Finco *et al*, Phys. Rev. Lett. **128**, 187201 (2022)] techniques. For each technique we will explain the operating principle, i.e. how the energy barrier imposed by the topological protection is overcome; specify the range of materials to which the technique applies to; and evaluate the advantages and disadvantages of the technique.

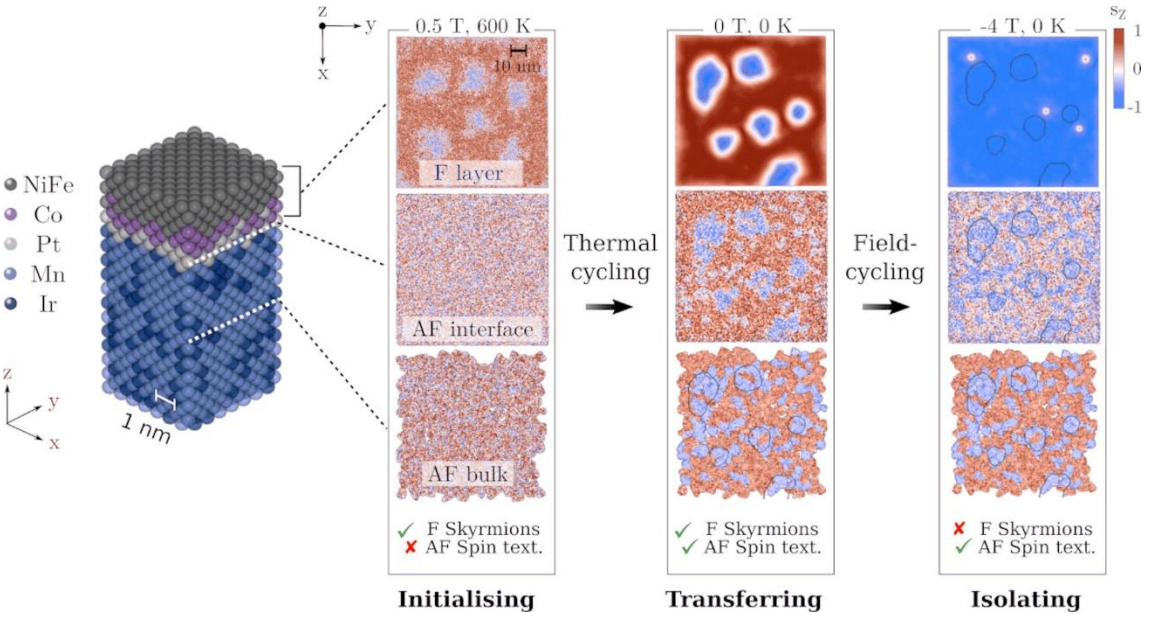


FIG. 3. Atomistic simulations showing the nucleation of localized spin textures in an antiferromagnet γ-$IrMn_3$, using the imprinting technique. Ferromagnetic skyrmions initialized in a $Ni_{80}Fe_{20}$/Co/Pt stack, optimized for the purpose, serve as a template for setting the underlying antiferromagnetic grains, due to the interfacial exchange interaction, during a thermal process. These localized antiferromagnetic textures can be isolated by applying an external field that annihilates the ferromagnetic skyrmions but leaves the antiferromagnetic textures intact. Adapted with permission from the American Physical Society: M. Leiviskä *et al*, Phys. Rev. B **108**, 184424 (2023). Copyright 2023.

Field-assisted nucleation techniques

Applying an external field to a magnetic system alters the energy balance and therefore can stabilize different magnetic textures. In ferromagnets, external field can overcome the energy barrier set by e.g. dipolar, magnetocrystalline, DMI interactions, and thus favor a uniformly aligned magnetic state. Intermediate fields, on the other hand, can allow magnetic domain formation and the nucleation of skyrmions in systems favoring chiral winding of the spins (optimal DMI – bulk or interfacial, exchange

stiffness, magnetocrystalline anisotropy) as was first demonstrated for bulk metallic MnSi [S. Muhlbauer *et al*, Science **323**, 915-919 (2009)] and bulk semiconducting $Fe_{1-x}Co_xSi$ [W. Munzer *et al*, Phys. Rev. B **81**, 041203(R) (2010)]. In antiferromagnets, the magnetic order parameter $\hat{\boldsymbol{L}}$ is less sensitive to the external fields and the coupling between the two is more complex due to the indirect coupling to $\hat{\boldsymbol{M}}_{net}$ [Eqs (5) and (6)]. Nevertheless, recent simulations have demonstrated the viability of field-assisted nucleation of antiferromagnetic skyrmions in various systems: in a triangular lattice antiferromagnet [H. Rosales et al., Phys. Rev. B 92, 214439 (2015)], in a bilayered antiferromagnet with layer-dependent staggered DMI-interaction [Hayami, Phys. Rev. B 105, 014408 (2022)], and in a two dimensional antiferromagnet with a general staggered magnetic field [Silva et al., Phys. Lett. A, 448, 128328 (2022)]. Experimental indications of such field-assisted nucleation, on the other hand, have been reported recently: the interfacial DMI in $Pt/Mn_3Sn$ heterostructures was shown to favor both antiferromagnetic skyrmion and meron nucleation, depending on the temperature [X. Liu *et al*, Adv. Mater. 35, 2211634 (2023)]. The use of interfacial engineering in stabilizing antiferromagnetic skyrmions and antiskyrmions was also explored in simulations [A. Mukherjee *et al*, Phys Rev B 105, 075102 (2022)]. Moreover, a fractional antiferromagnetic skyrmion lattice stabilized by the interplay between the anisotropic exchange couplings between the next-nearest neighbors and the applied external field has been experimentally observed in the insulating $MnSc_2S_4$ [S. Gao *et al*, Nature 586, 37 (2020)].

An alternative method of field-assisted nucleation of localized and pre-defined antiferromagnetic textures through imprinting from a ferromagnet has been demonstrated, both numerically [M. Leiviskä *et al*, Phys. Rev. B **108**, 184424 (2023)] and experimentally [G. Salazar-Alvarez *et al*, Appl. Phys. Lett. **95**, 012510 (2009) ; J. Wu *et al*, Nat. Phys. **7**, 303 (2011); K.G. Rana *et al*, Appl. Phys. Lett. **119**, 192407 (2021)]. This method utilises the interfacial exchange interaction in ferromagnetic/antiferromagnetic heterostructures [also responsible for the exchange bias, J. Nogues *et al*, J. Magn. Mag. Mat. 192 203 (1999)] to transfer spin textures nucleated in the ferromagnet to the antiferromagnet. Experimentally, this spin texture transfer or imprinting has been demonstrated with vortex states across the $Ni_{80}Fe_{20}$/γ-$IrMn_3$ interface [G. Salazar-Alvarez *et al*, Appl. Phys. Lett. **95**, 012510 (2009)] as well as the Fe/NiO and Fe/CoO interfaces [J. Wu *et al*, Nat. Phys. **7**, 303 (2011)], and with skyrmion-like bubbles across the ($Ni_{80}Fe_{20}$/Co/Pt)/γ-$IrMn_3$ interface [K.G. Rana *et al*, Appl. Phys. Lett. **119**, 192407 (2021)]. In the latter case, the interfacial parameters, such as DMI and perpendicular magnetic anisotropy, were optimized to favor interfacial skyrmion formation. In each of these experiments the spin textures were first nucleated in the ferromagnet with the aid of an external field, and then imprinted onto the antiferromagnet through a thermal process. This imprinting technique has been recently reproduced numerically, in search for antiferromagnetic skyrmions, using atomistic simulations (FIG. 3) [M. Leiviskä *et al*, Phys. Rev. B **108**, 184424 (2023)] to aid in the search for antiferromagnetic skyrmions. It was shown that upon imprinting, both the antiferromagnetic interface and the bulk adopt the ferromagnetic spin state while also showing signatures of the native spin state of the antiferromagnet. The main features, obtained using simulations, were also observed experimentally (see also §6 about the experimental methods to reveal antiferromagnetic skyrmions, and FIG. 8) [K.G. Rana *et al*, Appl. Phys. Lett. **119**, 192407 (2021)]. While the topological nature of the imprinted antiferromagnetic spin textures was not confirmed, this demonstration of the universal imprinting of various spin states is nevertheless a promising premise for further investigations of topological spin textures in antiferromagnets. Moreover, the possibility to isolate the antiferromagnetic spin textures [M. Leiviskä et al, Phys. Rev. B 108, 184424 (2023)] also opens up perspectives for their observation and studying their transport properties (§5) independently from the ferromagnetic template. Note, however, that the isolation requires an external field, which is not always compatible with *ad hoc* methods (§6).

Electrical nucleation techniques

For more scalable antiferromagnetic skyrmion devices relevant for practical applications, nucleation techniques by electrical means are most often more relevant than field-induced ones. Here we will discuss two such theoretically proposed techniques: one utilizing spin-polarized currents [X. Zhang *et*

*al*, Sci. Rep. **6**, 24795 (2016) ; C. Jin *et al*, Appl. Phys. Lett. **109**, 182404 (2016); K.I.A. Khan *et al*, Sci. Rep. 11, 12332 (2021)] and the other relying on the magnetoelectric effect [X. Xu *et al*, Phys. Rev. Appl. **11**, 024051 (2019)].

Injecting a spin-polarized current perpendicular to the plane (CPP) of an antiferromagnet can lead to switching of the magnetic moments through the action of spin-orbit torques [T. Jungwirth *et al*, Nature Nanotech. **11**, 231 (2016); V. Baltz *et al*, Rev. Mod. Phys. **90**, 015005 (2018)], which is the foundation for the use of spin-polarized CPP current in antiferromagnetic skyrmion nucleation. In antiferromagnetic systems for which parameters like the exchange stiffness and DMI strength have been optimized to favor skyrmion formation, atomistic dynamics simulations have shown that switching on, then off the CPP current may result in the system relaxing into the antiferromagnetic skyrmion ground state. In terms of device geometries, nanodisks [X. Zhang *et al*, Sci. Rep. **6**, 24795 (2016); K.I.A. Khan *et al*, Sci. Rep. **11**, 12332 (2021)], nanowires of fixed [C. Jin *et al*, Appl. Phys. Lett. **109**, 182404 (2016)], and variable cross-sectional size [X. Zhang *et al*, Sci. Rep. **6**, 24795 (2016)] have been considered. In the two former cases applying the CPP locally generates the antiferromagnetic skyrmion, when in the last case a pair of geometrically constrained antiferromagnetic domain walls is generated by the CPP current. This pair is then moved using current in plane-induced motion and subsequent spin-transfer torque, and it gradually deforms into an antiferromagnetic skyrmion upon crossing the constriction [FIG. 4(a)]. The nanowire geometries have the advantage of allowing current-induced motion of the antiferromagnetic skyrmions (see also §5). However, as proposed in the simulations, this requires a change in the direction in which the spin-polarized current is applied, which would then require a specific device architecture for experimental realization. We note that the electrical techniques discussed here are only applicable to conducting antiferromagnets, which limits the material range, contrary to the field-assisted and thermal/optical techniques as well as the technique discussed next. So far the reports on spin-polarized current-induced antiferromagnetic skyrmion nucleation are simulation-based, but a recent experimental work has demonstrated a generation of an antiferromagnetic half-skyrmion in CuMnAs upon subjecting the system to an (unpolarized) electric current pulse [O.J. Amin *et al*., Nat. Nanotechnology **18**, 849–853 (2023)]. This nucleation was attributed to a combined action of thermal and spin-torque effects.

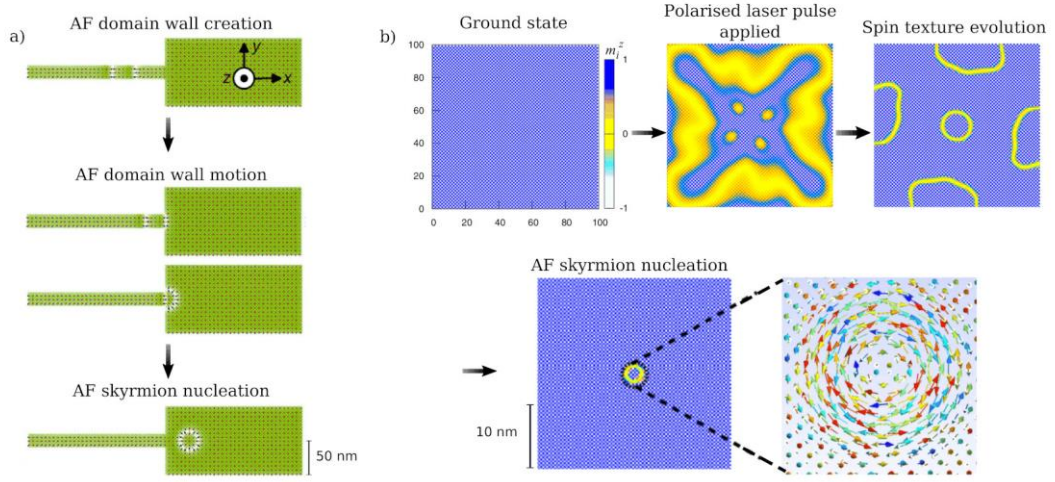


FIG. 4. Atomistic spin dynamics simulations illustrating the nucleation of an isolated skyrmion in a two-dimensional antiferromagnetic (a) nanotrack by a sequence of spin-polarized current – adapted from X. Zhang *et al*, Sci. Rep. **6**, 24795 (2016), CC BY license, and (b) insulator by an ultrafast laser pulse – adapted with permission from the American Physical Society: R. Khoshlahni *et al*, Phys. Rev. B 99, 054423 (2019). Copyright 2019.

In heterostructures containing a thin magnetic film and a non-magnetic film, the magnetic anisotropy is known to be sensitive to electric fields [R.-A. One *et al*, Sci. Rep. **11**, 8801 (2021); A.Fassatoui *et al*, Phys. Rev. Appl. **14**, 064041 (2020); A. Fassatoui *et al*, Small, 2102427 (2021); H. Terada *et al*, Sci. Rep. **7**, 5618 (2017)]. Therefore, applying an electric field to such a heterostructure can cause a rotation of the spins and in effect, allow a nucleation of skyrmions given that again the parameters such as the exchange stiffness and the DMI strength are optimized. This technique has been theoretically demonstrated to apply to both ferromagnetic and antiferromagnetic skyrmions [X. Xu *et al*, Phys. Rev. Appl. **11**, 024051 (2019)]. Note that this technique also enables erasing the skyrmion. The timescale for the antiferromagnetic skyrmion nucleation here is predicted to be of the order of 10 ps, which is two orders of magnitude faster than that of the ferromagnetic skyrmion nucleation.

Thermal and optical nucleation techniques

Finally, we will briefly cover the thermal and optical nucleation of antiferromagnetic skyrmions, which benefits from applicability to a wide range of systems beyond conducting materials and heterostructures, in contrast to some of the other mechanisms described. Moreover, it promises localized and ultrafast (sub ns) generation, both essential requirements for practical applications using antiferromagnetic skyrmions as information carriers.

Here the operating principle is that illumination by a laser pulse excites an ultra-thin antiferromagnetic insulator from its ground state to a local minimum containting a skyrmion, as illustrated in FIG. 4(b). The exact microscopic details can vary from thermal effects that generate sufficient thermal energy for overcoming the nucleation energy barrier [S.-G. Je *et al*, Nano Lett. **18**, 7362 (2018); G. Berruto *et al*, Phys. Rev. Lett. **120**, 117201 (2018); R. Juge *et al*, Nat. Commun. **13**, 4807 (2022)] to an effective magnetic field (generated by the optical inverse Faraday effect) that causes magnon excitations [R. Khoshlahni *et al*, Phys. Rev. B **99**, 054423 (2019); V. Flovik *et al*, Phys. Rev. B **96**, 140411(R) (2017)]. In these atomistic spin dynamics simulations, both the pulse width and the amplitude of the effective magnetic field have to be optimized in order to stabilize the antiferromagnetic skyrmion state. The latter can be manipulated through the application of a uniform magnetic field, which also affects the skyrmion size [R. Khoshlahni *et al*, Phys. Rev. B **99**, 054423 (2019)]. Experimentally, the formation of several skyrmions in the hundred nanometer range at the laser beam impact point has been observed in $[Pt(0.75)/Co(1.49)/Ru(0.85)]_6$ multilayer synthetic antiferromagnet [R. Juge *et al*, Nat. Commun. **13**, 4807 (2022)] and thin ferromagnetic films [S.-G. Je *et al*, Nano Lett. **18**, 7362 (2018) ; F. Büttner *et al*, Nat. Mater. **20**, 30 (2021)].

Finally, we note that in some antiferromagnetic systems topological defects can be native. For example, skyrmion formation has been inferred from the magnetotransport data in Li-doped $La_2CuO_4$, an insulating antiferromagnet, where the dopant geometry and character influence the magnetic texture formation [I. Raicevic *et al.*, PRL 106, 227206 (2011)]. Another example is the multiferroic $BiFeO_3$ that can host antiferromagnetic spin cycloids that have three equivalent propagation directions thus giving rise to different magnetic domains. At the boundaries of these domains topological defects have been observed [A. Finco *et al.*, Phys. Rev. Lett. 128, 187201 (2022)] [see also §6 and FIG. 7]. The interplay of these cycloids has been shown to also give rise to chiral magnetic textures across the ferroelectric domain walls [J.-Y. Chauleau *et al*., Nat. Mat. **19**, 386 (2020)]. In the insulating $\alpha$-$Fe_2O_3$, on the other hand, half-skyrmions and bimerons have been observed in the vicinity of the Morin transition [F. P. Chmiel *et al*, Nat. Mater. 17, 581 (2018) ; H. Jani *et al.*, Nature **590**, 74 (2021); . K. C. Tan *et al*, Nat. Mater. (2023)], where the favored spin orientation changes from in-plane to out-of-plane due to the temperature-dependent magnetocrystalline anisotropy. The stabilisation of these topological textures is essentially a consequence of the magnetic domain evolution across the Morin temperature.

## 5. Moving antiferromagnetic skyrmions: internal field-, thermal- and current-induced motions (RFLE, DG, JR, CC)

Much of the potential of antiferromagnetic skyrmions for applications in information storage and processing involves their dynamics under the action of forces arising from electrical currents, thermal gradients and localized changes to material properties such as DMI, anisotropy or exchange or even distortions of the skyrmion structure - so-called internal fields.

Current-induced motion

In the case of ferromagnetic skyrmions several sources of current-driven motion are often considered: (a) a spin Hall torque arising from an adjacent heavy metal (also referred in literature as spin-orbit torque), such as Pt (b) conventional spin-transfer torque and (c) a topological torque both arising from electron flowing along the magnetic texture shown schematically in FIG. 5(a).

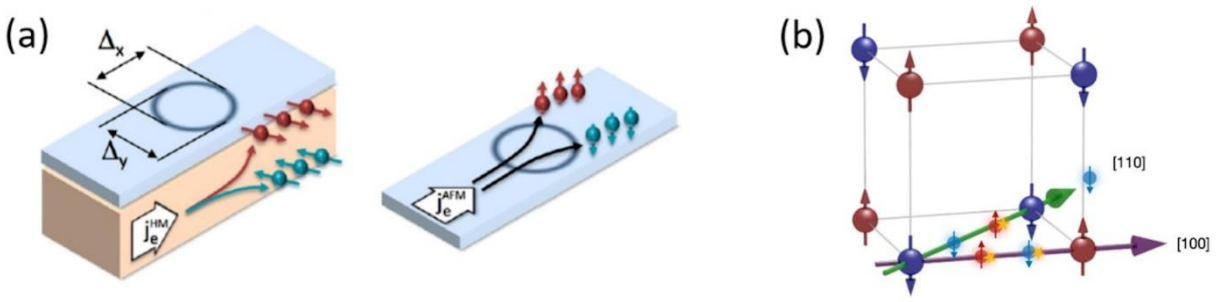


FIG. 5. (a) Illustration of typical geometries and corresponding physical effects considered in literature as possible sources for current-induced antiferromagnetic skyrmion dynamics: (left) spin Hall torque arising from an adjacent metal and (right) topological torque arising within antiferromagnets. Reprinted with permission from the American Physical Society: A. Salimath *et al*, Phys. Rev. B **101**, 024429 (2020). Copyright 2020. (b) Illustration of electron scattering in a simple antiferromagnetic material. Along certain crystal directions itinerant electrons "see" alternating or aligned local moments, leading to different scattering probabilities and crystalline anisotropic magnetoresistance. These can lead to sublattice resolved spin-transfer and spin-orbit torques along preferred directions, causing antiferromagnetic skyrmion motion.

In the case of antiferromagnetic skyrmions considered at the macroscopic scale, the opposite orientation of local magnetic moments naïvely leads to an averaging of spin-transfer and spin-orbit torques to zero. We therefore consider the origins of the forces on local magnetic moments with directions described by the unit vector $\boldsymbol{S}$. In a ferromagnet at low temperature the local magnetic moments are well-aligned with $\boldsymbol{S} \parallel \boldsymbol{M}$, while in an antiferromagnet the moments on alternating sublattices point in opposite directions $\boldsymbol{S}_{A,B} = \pm \boldsymbol{M}$. In both ferromagnetic and antiferromagnetic cases thermal and internal fields are additive and capable of driving skyrmions. For electrical currents the effects are more complicated. The current-induced driving force acting on any magnetic texture subjected to spin-polarized current results in the interaction between moving electron spins $\boldsymbol{s}$ and local magnetic moments $\boldsymbol{S}$. In the case when spins and magnetic moments are not collinear there is a transfer of angular momentum between two sub systems, which results in a torque seen by the magnetization. This torque is proportional to the cross product $\sim(\mathbf{S} \times \mathbf{s})$ between the local magnetic moments and the local direction of electron spins. Determining the magnitude of the torque is rather complicated and requires complex spin-transport calculations including details of the spatial spin distribution. The complexity means that in most situations attention is focused on the mutual

directions of magnetization and spin axes giving some uncertainty on the real spin-transfer amplitudes, which are adjusted by comparing with experimental data when it is available. In practice, the cross product $\sim(\mathbf{S}\times\mathbf{s})$ is decomposed in the plane tangent to the magnetization into two perpendicular axes giving so-called field-like torque and damping-like torque with adjustable prefactors [R. Msiska *et al*, Phys. Rev. Appl. **17**, 064015 (2022)]. For instance, in the case of spin Hall induced movement in FIG. 5(a), the corresponding torque acting on a magnetic moment takes the form

$$\boldsymbol{T}(S) = \varepsilon\boldsymbol{S}\times\left(\hat{\boldsymbol{z}}\times\boldsymbol{v}_{eff}\right) + \boldsymbol{S}\times\left[\boldsymbol{S}\times\left(\hat{\boldsymbol{z}}\times\boldsymbol{v}_{eff}\right)\right] \tag{10}$$

where $\varepsilon$ is the field-like to damping-like torque ratio, $\boldsymbol{v}_{eff}$ is the effective spin velocity and $\hat{\boldsymbol{z}}$ an axis perpendicular to the antiferromagnetic film.

The physical interaction of spins and local moments can be different in different device geometries, topological structures and materials and so the relative contributions of each term are often specific to certain situations. In ferromagnets the parallel alignment of local moments allows collective effects of torques that are able to naturally drive skyrmion motion. Macroscopically the alternating directions of the local moments on alternating sublattices in antiferromagnets mean that the spin-torques have opposite sign, and so either have no effect or are competing with the inter-sublattice exchange interactions (§3). Unlike ferromagnets, exciting the exchange mode can induce inertial dynamics and switching [A. V. Kimel *et al*, Nat. Phys. **5** 727(2009)] that can feasibly lead to skyrmion motion.

Despite this, most numerical studies consider collective torques that act in opposite directions on each magnetic sublattice [J. Barker & O. Tretiakov, Phys. Rev. Lett. **116**, 147203 (2016); C. Jin *et al*, Appl. Phys. Lett. **109**, 182404 (2016)]. At the microscopic level however the atomic structure plays an essential role in determining the strength of interactions with electrical currents, providing some insights into the physical origins of collective torques. Among the most notable materials with important symmetry are CuMnAs [P. Wadley *et al*, Sci. Rep. **5**, 17079 (2015)] and $Mn_2Au$ [V. Barthem *et al*, Nat. Commun. **4**, 2892 (2013)] which are planar antiferromagnets where the spins from each magnetic sublattice occupy complete planes. When applying currents parallel to the plane the currents are locally polarized leading to spin-transfer and spin-orbit torques [J. Železný *et al*, Phys. Rev. Lett. **113**, 157201 (2014)] enabling domain wall motion [S. Reimers *et al*, Nat. Commun. **14**, 1861 (2023)] and switching [P. Wadley *et al*, Science **351**, 587 (2016)]. This is due to the fact that electrons travelling parallel to each plane see local ferromagnetic order, allowing the appearance of coherent torques acting on each sublattice. The final situation is special symmetry planes, where collective spin-transport effects are possible. In the case of a simple cubic antiferromagnets, these would be along the (110) planes, while currents along the [100] and [111] directions would have only exchange effects FIG. 5(b). Another interesting class of compensated material are altermagnets, where electrical currents also interact differently with each magnetic sublattice depending on the current direction, albeit originating from non-relativistic physics [L. Smejkal et al, Phys. Rev. X **12**, 040501 (2022)]. Again different torques are then apparent on each sublattice, allowing collective motion of skyrmions.

Modelling of antiferromagnetic skyrmion dynamics is a developing field with few studies at present, unlike their ferromagnetic counterparts. Due to the complexity of their structure and interaction with internal and external forces (§3) predicting the dynamics of antiferromagnetic skyrmions is almost solely the domain of numerical simulations. The standard approach for modelling ferromagnets is numerical micromagnetics [C. Abert, Eur. Phys. J. B **92**, 120 (2019)] which treats nanoscale regions of a material as having a small and continuous change to the magnetization. The extension of micromagnetics to modelling antiferromagnetic systems is somewhat complex due to the large

(atomic-scale) exchange between sublattices, typically $H_E \sim 10 - 100\ T$ [U. Atxitia *et al*, Phys. Rev. B **86**, 104414 ( 2012); J. Hirst *et al*, Phys. Rev. B **106**, 094402 (2022); T. Moriyama *et al*, Phys. Rev. Mat. **7**, 054401 (2023)] and even then is only valid in the limit that the local sublattice magnetization changes slowly. Nevertheless some simulations of antiferromagnetic skyrmion dynamics driven by anisotropy gradients [L. Shen *et al*, Phys. Rev. B **98**, 134448 (2018)] and sublattice resolved torques [C. Jin *et al*, Appl. Phys. Lett. **109**, 182404 (2016)] provide some important insights into the qualitative dynamics. More accurate atomistic simulations [J. Barker & O. Tretiakov, Phys. Rev. Lett. **116**, 147203 (2016); E. A. Tremsina & G. S. D. Beach, Phys. Rev. B **106**, L220402 (2022); R. Khoshlahni *et al*, Phys. Rev. B **99**, 054423 (2019)] enable a more quantitative description of antiferromagnetic skyrmion dynamics due to their more exact representation of the inter-sublattice exchange interaction. However, atomistic models are much more computationally expensive and for simulating the large length and time-scales needed for skyrmion dynamics typically, a supercomputer is required. Despite their cost, the level of detail enables a significantly more accurate description of antiferromagnetic skyrmion dynamics and an intrinsic connection to crystal symmetry that is directly responsible for spin-torque effects. Multiscale models combining first principles parameterization, atomistic model simulations and a calibrated micromagnetic model provide a promising route to accurate simulations of antiferromagnetic skyrmions.

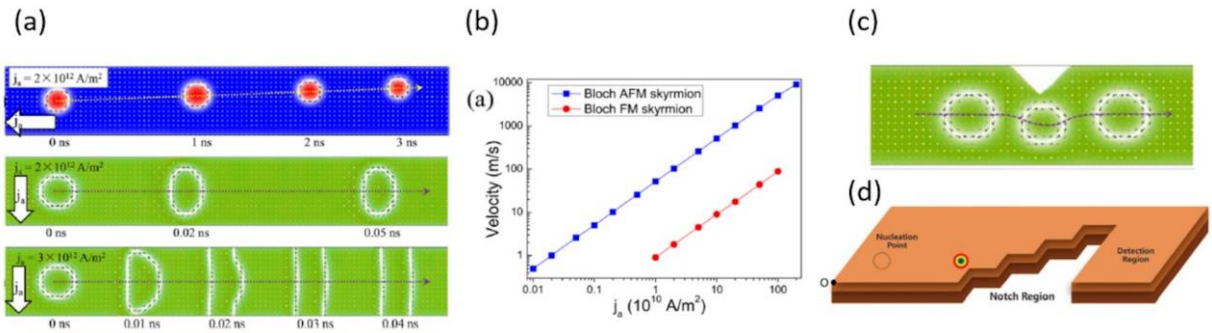


FIG. 6. (a) Comparison of motion of ferromagnetic skyrmion (blue nanotrack) and antiferromagnetic skyrmions (green nanotracks) driven by spin Hall induced driving force, obtained from simulations. (b) Corresponding comparison of antiferromagnetic (AFM) and ferromagnetic (FM) skyrmion velocities. (c) Illustration of antiferromagnetic skyrmion behaviour close to geometrical notch upon spin Hall induced dynamics. Adapted with permission from the American Institute of Physics: C. Jin *et al*, Appl. Phys. Lett. **109**, 182404 (2016). Copyright 2016. (d) Illustration of antiferromagnetic skyrmion-based diode. From N. Bindal *et al*, Nanoscale Adv. **5**, 450 (2023), CC BY license.

Although the number of tools to study antiferromagnetic skyrmion dynamics theoretically are limited at present and some methods used in literature go far beyond model applicability, we may still indicate some key features, which differentiate skyrmion current-induced dynamics in ferromagnets and antiferromagnets (see also §3 for an introduction). For instance, antiferromagnetic skyrmions have been shown to follow trajectories parallel to in-plane driving currents independently on the current-induced torque origin, in contrast to ferromagnetic skyrmions [FIG. 6(a)] [C. Jin *et al*, Appl. Phys. Lett. **109**, 182404 (2016); L. Shen *et al*, Appl. Phys. Lett. **114**, 042402 (2019); A. Salimath *et al*, Phys. Rev. B **101**, 024429 (2020)]. However, this finding has been recently questioned in [R. Msiska *et al*, Phys. Rev. Appl. **17**, 064015 (2022)], where authors emphasized extreme symplicity of previous models and shown situations for which Magnus forces acting on different antiferromagnetic skyrmion sub-lattices may not cancel giving rise to non-zero transverse velocity. Usually the numerical velocity of

antiferromagnetic skyrmions is proportional to the applied current amplitude and is reported to be around two orders of magnitude greater than that of ferromagnets [FIG. 6(b)] [X. Zhang *et al*, Sci. Rep. **6**, 24795 (2016) ; C. Jin *et al*, Appl. Phys. Lett. **109**, 182404 (2016) ; A. Salimath *et al*, Phys. Rev. B **101**, 024429 (2020)]. In addition to being related to the inter-sublattice exchange $H_E$, it may also be partly related to the fact that the skyrmion velocity is inversely proportional to the saturation magnetization $M_S$ due to inertial motion, as well as other material parameters such as exchange stiffness $A$ (absolute value) and anisotropy $K$.

Antiferromagnetic skyrmion displacement is usually accompanied by lateral deformation [FIG. 6(a)]. In A Salimath *et al*, Phys. Rev. B **101**, 024429 (2020), it has been demonstrated that this lateral expantion is proportional to the skyrmion velocity and is reminiscent of the well known Lorentz contraction identified in one-dimentional antiferromagnetic domain walls [O. Gomonay *et al*, Phys. Rev. Lett. **117**, 017202 (2016)]. The lateral expantion diverges when the skyrmion reaches the so-called spin wave velocity (which is of the order of few kilometers per second) and the skyrmion is stretched into two coherently moving domain walls. As topologically protected objects, antiferromagnetic skyrmions show high stability in the vicinity of any geometry modification such as edges or notches. In particular, the stability of an antiferromagnetic skyrmion and its ability to bypass obstacles make them promising objects for spintronic devices such as antiferromagnetic skyrmion-based high speed diode with processing speed in the order of $10^3$ m.s$^{-1}$[FIG. 6(d)], [N. Bindal *et al*, Nanoscale Adv. **5**, 450 (2023)].

Alternative sources for motion

In addition to current-induced antiferromagnetic skyrmion motion, several theoretical papers discuss alternative sources of driving forces. While the conventional method of employing electric currents to drive skyrmions remains prevalent, exploring alternative approaches to their manipulation is particularly intriguing, especially in the case of insulating antiferromagnets, where electric currents cannot flow.

By analogy with spin angular momentum transfer from electron sub-system to magnetic sub-system, the orbital angular momentum of phonons generates a torque on a magnetic texture. Thus, linear or circular surface acoustic waves may induce antiferromagnetic skyrmion motion [R. Khoshlahni *et al*, Phys. Rev. B **107**, 144421 (2023)]. In this case, the force vector in Eq. (9) is proportional to the difference in the angular momentum current between incident and scattered phonons. Interestingly, linear waves induce straight-line motion with zero Hall angle, whereas the difference in right and left phonon's orbital angular momentum current for circular waves gives rise to a ratchet motion. Numerical simulations estimate that, in the presence of surface acoustic waves, antiferromagnetic skyrmions can reach a maximum velocity of 250 m.s$^{-1}$.

Another alternative method is to apply a voltage-controlled magnetic anisotropy gradient to the insulating antiferromagnetic texture, and in particular the linear gradient of a perpendicular magnetic anisotropy constant K along the direction of propagation [L. Shen *et al*, Phys. Rev. B **98**, 134448 (2018)]. According to the voltage sign the antiferromagnetic moves either towards the area with lower or higher magnetic anisotropy. In contrast to ferromagnetic skyrmion which moves perpendicular to the gradient direction, antiferromagnetic skyrmions move along the gradient. Theoretical calculations suggest that the magnetic anisotropy gradient can promote velocities up to 500 m.s$^{-1}$, which is comparable to that of ferromagnetic skyrmions.

Thermal gradients may also be considered as the driving force source [R. Khoshlahni *et al*, Phys. Rev. B **99**, 054423 (2019)]. Stimulation of magnons in antiferromagnetic insulators by applying a thermal gradient to the system may cause the skyrmions motion in a longitudinal direction with zero Hall angle. In this case, the resulting skyrmion velocity includes two contributions with opposite signs: magnon-

induced contribution and stochastic Brownian motion contribution. The size of the skyrmion may influence the resulting direction of movement by favoring one or another term.

In general numerical simulations are somewhat ahead of experiments in the field of $m.s^{-1}$ skyrmions due to the difficulty in measuring them, resolving their ultrafast dynamics, and accurate material characterization. However, most simulations so far are qualitative in nature and will need significant advancement over the coming years. In particular, detailed first-principles calculations of the interaction of spin currents and antiferromagnetic materials are needed to parameterize more approximate models suitable for atomistic and micromagnetic calculations. Materials science also plays a critical role in developing realistic numerical models, including correct crystal structures, model parameters validated against experiment and the inclusion of multiple magnetic sublattices for non-collinear antiferromagnetic systems. Further developments in multiscale models should also enable larger-scale calculations, while advancing computing power will enable more accurate atomistic models to be widely employed.

## 6. Detecting antiferromagnetic skyrmions: magnetic, optical, thermal and electrical techniques (VB, SJ)

In this section, we present examples of techniques that have been tried and tested or that are under study in antiferromagnetic spintronics [V. Baltz *et al*, Rev. Mod. Phys. **90**, 015005 (2018); S.-W Cheong *et al*, npj Quantum Mater. **5**, 3 (2020)]. Some of these techniques should enable the study of both static and dynamic behaviour in antiferromagnetic skyrmions, and, in some cases, offer the possibility to measure the information in future devices based on antiferromagnetic skyrmions.

Since antiferromagnets lack a net magnetization the experimental observation and nucleation of their skyrmions is challenging. Nevertheless, the direct observation of antiferromagnetic spin textures in general can be achieved, but only in large-scale facilities with element-sensitive techniques like X-ray absorption spectroscopy [N. B. Weber *et al*, Phys. Rev. Lett. **91**, 237205 (2003) ; G. Salazar-Alvarez *et al*, Appl. Phys. Lett. **95**, 012510 (2009); J. Wu *et al*, Nat. Phys. **7**, 303 (2011); K. G. Rana *et al*, Appl. Phys. Lett. **119**, 192407 (2021); O. J. Amin *et al*, Nature Nanotech. **18**, 849 (2023)], specific local probe techniques such as spin-polarized scanning tunneling microscopy [M. Bode *et al*, Nat. Mater. **5**, 477 (2006); S. Loth *et al*, Science **335**, 196 (2012)], and quantum sensing with single spins (nitrogen-vacancy) in diamond [I. Gross *et al*, Nature **549**, 252 (2017); T. Kosub *et al*, Nature Commun. **8**, 13985 (2017) ; M. S. Wörnle *et al*, arXiv:1912.05287 (2019) ; J.-Y. Chauleau *et al*, Nat. Phys. **19**, 386 (2020); A. Finco *et al*, Nature Commun. **12**, 767 (2021); A. Finco *et al*, Phys. Rev. Lett. **128**, 187201 (2022)], or optical second harmonic generation [M. Fiebig *et al*, Phys. Rev. Lett. **87**, 137202 (2001); J.-Y. Chauleau *et al*, Nat. Mater. **16**, 803 (2017)], thermal gradient microscopy [H. Reichlova *et al*, Nat. Commun. **10**, 5459 (2019)] and magneto-optical Kerr miscoscopy [T. Higo *et al*, Nature Photonics **12**, 73 (2018)]. Antiferromagnetic domains and domain walls in NiO [M. Fiebig *et al*, Phys. Rev. Lett. **87**, 137202 (2001); N. B. Weber *et al*, Phys. Rev. Lett. Lett. **91**, 237205 (2003)], $BiFeO_3$ [I. Gross *et al*, Nature **549**, 252 (2017); J.-Y. Chauleau *et al*, Nat. Mater. **16**, 803 (2017)], $Cr_2O_3$ [T. Kosub *et al*, Nature Commun. **8**, 13985 (2017)], CuMnAs [M. S. Wörnle *et al*, arXiv:1912.05287 (2019)] and $Mn_3Sn$ [T. Higo *et al*, Nature Photonics **12**, 73 (2018) ; H. Reichlova *et al*, Nat. Commun. **10**, 5459 (2019)], vortex states in IrMn [G. Salazar-Alvarez *et al*, Appl. Phys. Lett. **95**, 012510 (2009)] and NiO [J. Wu *et al*, Nat. Phys. **7**, 303 (2011)] layers, and other types of textures in $BiFeO_3$ [J.-Y. Chauleau *et al*, Nat. Phys. **19**, 386 (2020); A. Finco *et al*, Nature Commun. **12**, 767 (2021)] and IrMn [K. G. Rana *et al*, Appl. Phys. Lett. **119**, 192407 (2021); M. Leiviskä *et al*, Phys. Rev. B 108, 184424 (2023)] were investigated in those ways in search for antiferromagnetic skyrmions. Recently, fractional antiferromagnetic skyrmion lattices in bulk $MnSc_2S_4$

were observed at cryogenic temperature using neutron scattering experiments [S. Gao *et al*, Nature **586**, 7827 (2020)] as well as antiferromagnetic half-skyrmions and bimerons in $\alpha$-$Fe_2O_3$ [F. P. Chmiel *et al*, Nat. Mater. 17, 581 (2018) ; H. Jani *et al*, Nature **590**, 74 (2021); . K. C. Tan *et al*, Nat. Mater. (2023)] and CuMnAs at room temperature [O. J. Amin *et al*, Nature Nanotech. **18**, 849 (2023)].

We recall that the important bottleneck, prior to any observation, remains the nucleation of skyrmions in thin films of antiferromagnets at room temperature, as discussed in §4, this is the current priority milestone for this field of research.

The presence of a spin texture in a uniformly magnetized surrounding will create magnetic stray fields near the material's surface, even though an antiferromagnet has no net magnetisation. This will most often be enhanced by the presence of uncompensated moments displaying a non-zero magnetization $\boldsymbol{M}$ - these same moments are the ones used, for example, for nucleating an antiferromagnetic texture through imprinting from an exchange coupled ferromagnetic skyrmion [K. G. Rana *et al*, Appl. Phys. Lett. **119**, 192407 (2021); M. Leiviskä *et al*, Phys. Rev. B 108, 184424 (2023)] (§4).

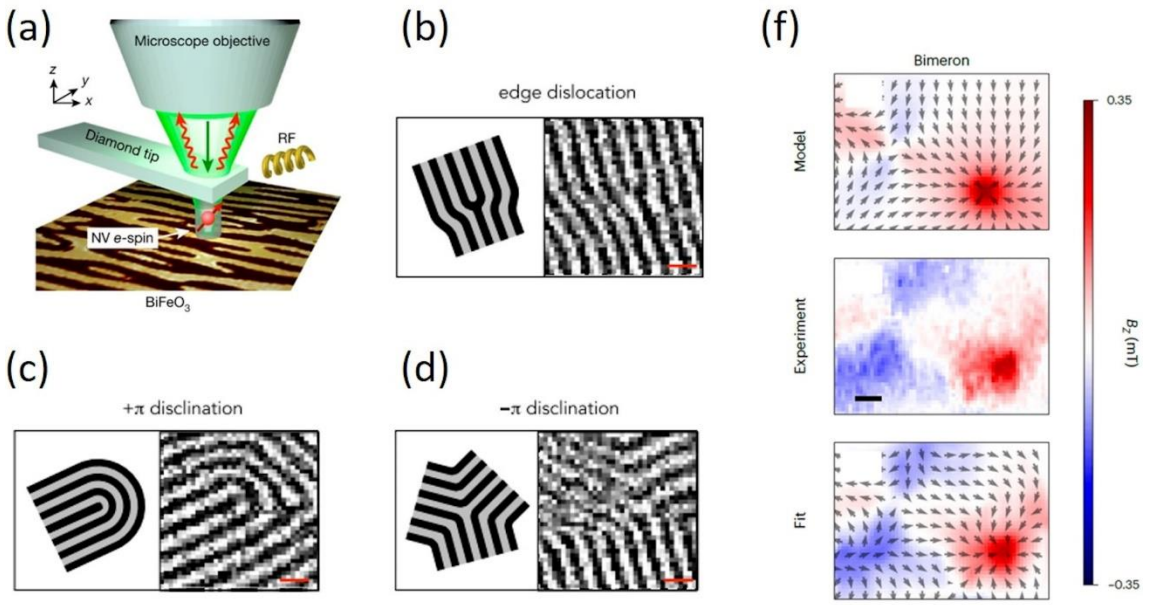


FIG. 7. (a) Illustration of scanning magnetic microscopy based on single-spin magnetometry, using the unique optical and spin properties of a nitrogen-vacancy (NV) centre in a diamond tip. Reprinted with permission from Springer Nature: I. Gross *et al*, Nature **549**, 252 (2017). Copyright 2017. (b-d) Sketches and corresponding images of several types of antiferromagnetic textures (though not skyrmions) in $BiFeO_3$, obtained by scanning magnetic microscopy based on NV single-spin magnetometry. The scale bar indicates 100 nm. Reprinted with permission from the American Physical Society: A. Finco *et al*, Phys. Rev. Lett. **128**, 187201 (2022). Copyright 2022. (e) Bimeron observed by NV-magnetometry in the canted easy plane antiferromagnet $\alpha$-$Fe_2O_3$, above the Morin transition, and corresponding model and fit. Adapted from A. K. C. Tan et al, Nat. Mater. (2023), DOI:10.1038/s41563-023-01737-4, CC BY license.

Magnetometry and relaxometry

Scanning magnetic microscopy based on single-spin magnetometry using a nitrogen-vacancy centre in diamond tips [FIG. 7(a)] is particularly well suited to detecting the small stray fields from antiferromagnetic textures [A. Finco and V. Jacques, arXiv:2307.06730 (2023)]. The unrivalled

combination of magnetic field sensitivity (~µT) and spatial resolution (~20 - 40 nm) should make it possible to provide quantitative static snapshot images of the distribution of the magnetic field created by an antiferromagnetic skyrmion, in the same way as has been done, for example, to image antiferromagnetic domains walls [I. Gross *et al*, Nature **549**, 252 (2017); T. Kosub *et al*, Nature Commun. **8**, 13985 (2017)] and antiferromagnetic topological defects [FIG. 7(b-d)] [J.-Y. Chauleau *et al*, Nat. Phys. **19**, 386 (2020); A. Finco *et al*, Phys. Rev. Lett. **128**, 187201 (2022); A. K. C. Tan *et al*, Nat. Mater. (2023)]. When the magnetic stray field is too small for the capacities of single-spin magnetometry, the same tool can be used in relaxometry mode [B. Flebus and Y. Tserkovnyak, Phys. Rev. Lett. **121**, 187204 (2018)]. This mode is based on the coupling between the spin angular momentum of the nitrogen-vacancy centre and the surrounding angular momentum, including magnons in the presence of an antiferromagnetic texture, which is a source of magnetic noise. This coupling alters the spin relaxation time of the nitrogen-vacancy centre, which can be measured, as proof-tested to image domain walls of a synthetic antiferromagnet [A. Finco *et al*, Nature Commun. **12**, 767 (2021)].

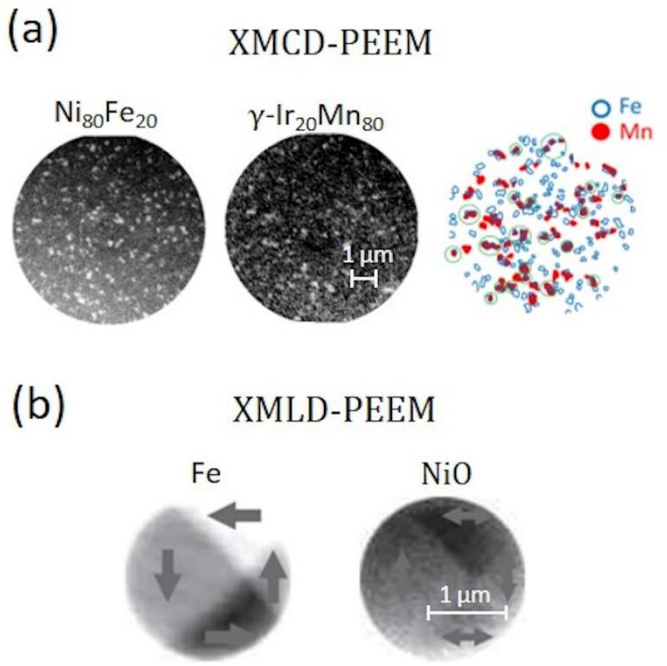


FIG. 8. (a) Ferromagnetic Néel-type skyrmion in NiFe (see §2 and §3), and resulting textures at the interface of an IrMn antiferromagnet, after attempting replication, in search for antiferromagnetic skyrmions, using the technique described in §4, observed by x-ray magnetic circular dichroism photoemission electron microscopy (XMCD-PEEM). Adapted with permission from the American Institute of Physics: K. G. Rana *et al*, Appl. Phys. Lett. **119**, 192407 (2021). Copyright 2021. (b) Ferromagnetic antimeron, with $(p_F, m_F, \gamma_F) = (1/2, 1, \pi/2)$ (see §2 and §3), in a patterned disc of Fe, and its replication across a 0.6 nm-thick NiO antiferromagnet, using the technique described in §4, observed by x-ray magnetic linear dichroism photoemission electron microscopy (XMLD-PEEM). Adapted with permission from Springer Nature: J. Wu *et al*, Nat. Phys. **7**, 303 (2011). Copyright 2011. See for example N. Gao et al, Nature Commun. 10, 5603 (2019) for the correspondance between meron/antimeron and vortex/antivortex.

X-ray optics

Some X-ray optics techniques also stand as viable solutions to resolve antiferromagnetic skyrmions. Combining x-ray magnetic circular dichroism (XMCD) with photoemission electron microscopy (PEEM), and taking advantage of the element sensitivity of the technique coupled with its spatial resolution of ~25 nm, allows imaging the magnetization $\boldsymbol{M}$ resulting from uncompensated moments sitting at the surface or interface of antiferromagnetic textures [FIG. 8(a)] [G. Salazar-Alvarez *et al*, Appl. Phys. Lett. **95**, 012510 (2009); K. G. Rana *et al*, Appl. Phys. Lett. **119**, 192407 (2021)]. The analog technique using linear dichroism (XMLD-PEEM) allows for probing the direction of the Néel vector $\boldsymbol{L}$, as integrated from the surface to the core of the material [FIG. 8(b)] [F. P. Chmiel *et al*, Nat. Mater. 17, 581 (2018) ; J. Wu *et al*, Nat. Phys. **7**, 303 (2011); H. Jani *et al*, Nature **590**, 74 (2021) ; O. J. Amin *et al*, Nature Nanotech. **18**, 849 (2023)]. One of the advantages of X-ray optics compared to scanning magnetic microscopy based on single-spin magnetometry and relaxometry is the possibility of time resolution (~0.1 ns) [V. López-Flores *et al*, J. Phys.: Condens. Matter **32**, 465801 (2020)], which opens up prospects for the study of the dynamic properties of antiferromagnetic skyrmions.

Magneto-thermoelectric microscopy

Magneto-thermoelectric microscopy using a laser [H. Reichlova *et al*, Nature Commun. **10**, 5459 (2019)], have been implemented to image antiferromagnetic domains in materials like $Mn_3Sn$, which exhibits some anomalous Nernst effect, the thermal analog of the anomalous Hall effect. However, this technique is limited by the optical diffraction limit. The demonstration that inducing a local temperature gradient by the contact of an atomic force microscope tip can allow magneto-thermoelectric microscopy with high spatial resolution [H. Isshiki *et al*, Front. Phys. **11**, 1205556 (2023)] now makes this type of techniques a viable solution for imaging antiferromagnetic skyrmions, for which the topological Hall effect should be accompanied by a topological Nernst effect, in a similar way to ferromagnetic skyrmions [M. Hirschberger *et al*, Phys. Rev. Lett. **125**, 076602 (2020)].

While the techniques presented above will provide a better understanding of antiferromagnetic skyrmions and their dynamic properties, electrical techniques, relying on the topological spin Hall effect [P. M. Buhl *et al*, Phys. Status Solidi RRL **11**, 1700007 (2017); C. Akosa *et al*, Phys. Rev. Lett. **121**, 097204 (2018)] and topological Hall effect [B. Göbel *et al*, Phys. Rev. B **96**, 060406(R) (2017)], which are both predicted to be non-necessarily zero in antiferromagnetic skyrmions [see also §3 and FIG. 2(b)], are the most viable for applications. See also R. Msiska *et al*, Phys. Rev. Appl. **17**, 064015 (2022) for the reciprocal skyrmion Hall effect in some antiferromagnets, which can be made non-zero due to the helicity-dependence of the forces $\boldsymbol{F}$ acting on the sublattices when initiated by spin-orbit torque [Eqs. (4) and (9) and corresponding text. Experimental verification of theoretical predictions on the influence of an antiferromagnetic skyrmion on electron dynamics is a priority pending.

## 7. Conclusion and perspectives (VB, RFLE)

In this chapter, we reviewed the specific features associated with the skyrmion topological object in antiferromagnetic materials, from the point of view of both magnetic and electrodynamic properties, in the context of possible applications.

Due to its antiferromagnetic nature, a skyrmion in an antiferromagnetic material, i. e. an antiferromagnetic skyrmion, has naturally no net magnetization, making it robust against external magnetic fields. This is a first natural advantage over ferromagnetic equivalents, for applications where magnetic integrity is required.

When the magnetic texture of the simplest antiferromagnetic and ferromagnetic skyrmions can be described in a similar manner, the dynamics of the order parameter significantly differs (§2, 3, 5): i) the motion of an antiferromagnetic skyrmion is in the THz range, as the exchange field, $H_E$, is several orders of magnitude greater than the terms such as anisotropy and dipolar fields that usually govern ferromagnetic dynamics, which is in the GHz range. This opens the way to the use of antiferromagnetic skyrmions as ultrafast information carriers. ii) The motion of an antiferromagnetic skyrmion follows inertial or Newtonian kinetics, due to intersublattice interactions causing feedback dynamics, opening up prospects for manipulation by ultrashort stimuli. Moreover, using antiferromagnets is a priori foreseen as a possible solution for mitigating the skyrmion Hall effect (§2, 3, 5). This effect is ascribed to the interaction between the electron flow and the topology of the magnetic object, resulting in the lateral deviation of most ferromagnetic skyrmions from the electron flow. It is undesirable in planned spintronic applications as it will lead to limitations in the propagation of spin information, e. g. through annihilation at the edges after a certain distance. For the case of the simplest bipartite antiferromagnetic skyrmions the transverse forces acting on the two imbricated ferromagnetic sublattices are assumed to be self-compensating. The reality is somewhat more subtle and calls for caution (§2, 3, 5). For example, the texture of a skyrmion in itself, even in the case of the simplest bipartite antiferromagnet is not necessarily trivial and some non-zero net transverse forces can be restored, especially when the helicity $\gamma_{AF}$ is non-zero. The inherent magnetic order of an antiferromagnet may also be more complicated, beyond collinear bipartite antiferromagnets in which case other descriptions, like cluster multipole moments is more appropriate, and may give rise to more subtle kinetics. Moreover an antiferromagnetic skyrmion is not necessarily a two-dimensional object, but may well extend along the third dimension, i. e. a tubular skyrmion or a bobbler. The fine texture of the skyrmion along the third dimension will certainly influence its motion and modify the fine tuning anticipated in two-dimensions for mitigating the skyrmion Hall effect. We also note that some pinning on defects or certain spin torque geometries can modify the morphology of the skyrmion, thus influencing its motion. This needs to be taken into account, by use of atomistic models, which are relevant to tackle interactions at the atomic level, like antiferromagnets call for, beyond simplistic macroscopic approximations. Accurately accounting for transport parameters in such atomistic simulations, beyond phenomenological models, is yet another ongoing challenge for the community, in order to compute accuratly transfer of angular momentum across interfaces in heterostructures making use of antiferromagnetic skyrmions, for a better guidance of applications (§5).

Conversely, the influence of an antiferromagnetic skyrmion on electrodynamics has long been hampered by the incorrect belief that a collinear bipartite antiferromagnetic skyrmion does not exhibit a net skyrmion Hall effect and therefore would not cause a reciprocal topological Hall effect, although a topological spin Hall effect is possible (§2, 3). Demonstrations that antiferromagnetic skyrmions can exhibit a net skyrmion Hall effect and that a collinear bipartite antiferromagnetic skyrmion crystal with non-equivalent sub-lattice sites can exhibit a non-zero topological Hall, opened perspectives for the electrical detection of antiferromagnetic skyrmions in spintronic devices.

Controlled and reproducible experimental nucleation of antiferromagnetic skyrmions is a critical step in further investigations of their properties as well as in their implementation in practical applications (§4). Controlling the order parameter of compensated magnets, however, is not trivial due to it being weakly sensitive to external field perturbations. Therefore, the experimental work is very fragmented and at its infancy, making experimental nucleation of antiferromagnetic skyrmion in thin films the priority milestone, for which a variety of magnetic, electrical, thermal and optical techniques are hopefully proposed (§4). The good point though is that some of these techniques: magnetic, optical, thermal and electrical, that have been tried and tested or that are under study in the more general context of antiferromagnetic spintronics should enable the study of both static and dynamic

behaviour, under the influence of field, temperature, light and current-induced, in antiferromagnetic skyrmions, and, in some cases, offer the possibility to measure the information in future devices based on antiferromagnetic skyrmions (§6).

In general numerical simulations (§5) are somewhat ahead of experiments in the field of antiferromagnetic skyrmions due to the difficulty in measuring them, resolving their ultrafast dynamics, and accurate material characterization. However, most simulations so far are qualitative in nature and will need significant advancement over the coming years. In particular, detailed first-principles calculations of the interaction of spin currents and antiferromagnetic materials are needed to parameterize more approximate models suitable for atomistic and micromagnetic calculations. Materials science also plays a critical role in developing realistic numerical models, including correct crystal structures, model parameters validated against experiment and the inclusion of multiple magnetic sublattices for non-collinear antiferromagnetic systems. Further developments in multiscale models should also enable larger-scale calculations, while advancing computing power will enable more accurate atomistic models to be widely employed.

There are a few related areas of development that could also aid understanding and technological innovation in the field of skrymions in magnetically compensated magnets. Altermagnetism [L. Smejkal et al, Phys. Rev. X **12**, 040501 (2022)] is the obvious candidate where a material presents a compensated magnetic phase combined with some spin-polarization. This would possibly lead to some sublattice-resolved coupling effects allowing the driving of the skyrmions with electrical currents. Materials with reduced dimensionality considering 2D and 2.5D (ultrathin films of a few monolayers) magnets are interesting as they can significantly change the dynamic and static propeties of domain walls and topological structures [I. M. Alliati *et al*, npj Comput. Mat. **8**, 3 (2022)], leading to enhanced stability. In the initial stages synthetic antiferromagnetic skyrmions [W. Legrand *et al*, Nat. Mater. **19**, 34 (2020)] could be interesting as their exchange fields are weak, but they can be engineered in a wide range of materials and benefit from inertial dynamics. However, the weak antiferromagnetic exchange coupling (arising from interlayer exchange coupling) means that the velocities are only a little higher than ferromagnetic skyrmions limiting their true potential as ultrafast information carriers. A final set of materials are ferrimagnets [S. K. Kim *et al*, Nat. Mater. **21**, 24 (2022)], presenting a net magnetic moment but also possessing antferromagnetic sublattice coupling. Like ferromagnets, these suffer from the skyrmion Hall effect, but can also be compensated making them effectively antiferromagnetic with zero net magnetic moment, but possessing non-zero spin angular momentum.

**Acknowledgments**

This study was supported by the Alliance Hubert Curien international programme (PHC) 'ASK' (Grant No. 46298XC), the CNRS international research project (IRP) 'CITRON', and the EPSRC international networking programme (Grant No. EP/V007211/1).